



Homogeneous photoconversion of seawater uranium using copper and iron mixed-oxide semiconductor electrodes



Seunghoon Lee^{a,b}, Unseock Kang^{a,b}, Guangxia Piao^{a,b}, Soonhyun Kim^c, Dong Suk Han^d, Hyunwoong Park^{a,b,e,*}

^a School of Energy Engineering, Kyungpook National University, Daegu 41566, Republic of Korea

^b School of Architectural, Civil, Environmental, Energy Engineering, Kyungpook National University, Daegu 41566, Republic of Korea

^c Division of Nano and Energy Convergence Research, Daegu Gyeongbuk Institute of Science and Technology, Daegu 42988, Republic of Korea

^d Chemical Engineering Program, Texas A&M University at Qatar, Education City, Doha, P.O. Box 23874, Qatar

^e Advanced Institute of Water Industry, Kyungpook National University, Daegu 41566, Republic of Korea

ARTICLE INFO

Article history:

Received 9 September 2016

Received in revised form 9 January 2017

Accepted 2 February 2017

Available online 3 February 2017

Keywords:

Photoelectrochemical
Resource recovery
Electron shuttle
p-type
Nuclear waste

ABSTRACT

Sunlight-driven conversion of hexavalent uranium (U(VI)) in seawater is achieved with mixed p-type CuO and CuFeO₂ (CuO/CuFeO₂) photocatalyst film electrodes synthesized via electrodeposition (ED) of Cu(II) and Fe(III), followed by annealing in air. The mixed photocatalysts exhibit a double-layer configuration with crystalline structures of CuO and CuFeO₂. On irradiation of the CuO/CuFeO₂ electrodes (held at –0.5 V vs. SCE) with solar simulated light (air mass 1.5; 100 mW cm⁻²), the U(VI) concentration decreases with time, while the total amount of uranium in solution does not change. This indicates that virtually all conversion reactions of U(VI) occur in the bulk solution, while surface reactions are limited due to insignificant adsorption of U(VI). U(VI) conversion leads to the mixed production of lower oxidation states U⁴⁺, U^{14/3+}, and U^{16/3+} at a ratio of 42:28:30, with an overall Faradaic efficiency of ~98%. The kinetics and induction time for U(VI) conversion are significantly influenced by the conditions of photocatalyst synthesis (CuO/CuFeO₂, CuO, and CuFeO₂; ED times of 2–4 h), the applied potential value (–0.4, –0.5, and –0.6 V vs. SCE), and the seawater condition (air-equilibrated vs. N₂-purged; pH 3–10.4). Based on the obtained results, O₂ is proposed to play a key role in shuttling photogenerated electrons between the electrodes and U(VI). In addition, the existence of an induction time is discussed in terms of material and reaction pathway.

© 2017 Elsevier B.V. All rights reserved.

1. Introduction

As carbon-neutral energy has emerged as the key to the sustainable growth of global communities, nuclear power has received growing attention worldwide [1–3]. Despite the long debate on safety and impact on the natural environment and human societies, nuclear power is still considered an alternative to fossil-fuel-based power because of its immediate CO₂ mitigation, both nationally and internationally. Uranium, a primary nuclear fuel, is a relatively common element in the Earth's crust and is traded securely under scrutiny [3–5]. Nevertheless, increases in the demand for energy security and political conflicts revisit the sustainability of the traditional supply chain.

In this regard, seawater uranium has received renewed attention in terms of securing the uranium supply because of its vast amount in oceans (45×10^8 ton, ~1000 times the territorial reservoir). Although the natural uranium concentration in seawater is as low as ~3 ppb [3], its uniform distribution in oceans encourages the development of recovery technology. The most common recovery process is the traditional sorption of U(VI), which exists as hydroxyl-carbonated uranyl anions (e.g., $(\text{UO}_2)_2(\text{OH})_3\text{CO}_3^-$ and $\text{UO}_2(\text{CO}_3)_3^{4-}$), in air-equilibrated seawater at pH ~8.2, using various sorbents, including amidoxime [6], oxides [7,8], polymers [6,9], and sediments [10]. Sorption recovery is practical and promising; however, it does not change the oxidation states of U(VI). Considering that UO₂ is the favored chemical form for nuclear power operations, the recovered U(VI) requires post-chemical conversion for further utilization as a fuel. To address this challenge, photocatalytic recovery and simultaneous conversion of U(VI) using TiO₂ have often been studied [11–14]. However, most studies were performed in deionized water or well-controlled aqueous media,

* Corresponding author at: School of Energy Engineering, Kyungpook National University, Daegu 41566, Republic of Korea.

E-mail address: hwp@knu.ac.kr (H. Park).

which limits insight into the photoconversion mechanism in real seawater.

Recently, we reported the photoelectrochemical recovery and simultaneous conversion of U(VI) in seawater using porous TiO₂ film electrodes [15]. Under simulated sunlight irradiation, U⁶⁺ underwent stepwise reduction to U⁴⁺³⁺ and U⁴⁺ (coordinated to oxygen) in an 8:2 ratio on the TiO₂ electrode surface; seawater has a similar uranium composition. The Faradaic efficiency of the uranium reduction was estimated at nearly 100%, with most reactions occurring on the TiO₂ surface (~95% of total uranium). However, the use of TiO₂ raises some technical issues. Firstly, TiO₂ is an n-type semiconductor with the valence and conduction bands bent downwards. Therefore, TiO₂ is not appropriate for direct injection of the majority carriers (*i.e.*, electrons) to the interfacial solution. An application of negative bias can induce upward bending of the bands, leading to an overlap between the Fermi level and the conduction band edge. Secondly, the distribution of uranium on the surface and in solution, requires additional post-separation and collection steps. It would be more practical if reduced uranium accumulated in one phase (surface vs. solution).

With this in mind, we attempted to convert seawater uranium using mixed p-type CuO and p-type CuFeO₂ (CuO/CuFeO₂; CFO) film electrodes. CFO is composed of earth-abundant elements and possesses a suitable energy level configuration capable of efficiently transferring photogenerated electrons to interfacial acceptors. Both the semiconductors have often been used for reduction reactions in non-saline aqueous media [16,17]. In this study, we have explored the applicability of mixed p-type electrodes to seawater uranium photoconversion.

2. Experimental section

2.1. Fabrication of photoelectrodes

Mixed CuO and CuFeO₂ electrodes (CuO/CuFeO₂; CFO) were fabricated on fluorine-doped SnO₂ (F:SnO₂, FTO) soda lime glass (Pilkington, ~50-nm-thick FTO layer) *via* electrodeposition, as reported elsewhere [16]. In brief, FTO substrates (1.5 cm × 3 cm; active area exposed to solution ~0.78 cm²) were placed in aqueous perchlorate solution (KClO₄, 50 mM, Aldrich) containing Cu(NO₃)₂·3H₂O (4 mM, Aldrich) and Fe(ClO₄)₃·H₂O (12 mM, Aldrich). They were then held at -0.36 V vs. SCE (saturated calomel electrode) for 2 h by a potentiostat/galvanostat (CompactStat, Ivium). A platinum gauze was used as the counter electrode. After drying in air, the as-deposited samples were annealed at 650 °C for 3 h in air. For comparison, CuFeO₂ electrodes were also fabricated by annealing the as-deposited samples at 650 °C for 2 h under an Ar atmosphere. For the fabrication of CuO electrodes, electrodeposition was performed in aqueous perchlorate solution with Cu(NO₃)₂·3H₂O (4 mM, Aldrich), followed by annealing at 650 °C for 2 h under an air atmosphere.

2.2. Photoelectrochemical seawater uranium conversion

Hexavalent uranium (U(VI)) stock solutions (30 or 100 ppm) were prepared weekly by dissolving uranyl nitrate (UO₂(NO₃)₂·6H₂O, purity >98.0%, Sigma Aldrich) in natural seawater derived from the East Sea, Korea (latitude: 36.13°, longitude: 129.40°). Before using, the sampled seawater was filtered through 0.45-μm PTFE membranes (Millipore) to remove particulate matter. Detailed information on the ionic composition of seawater is available elsewhere [15]. CFO, SCE, and Pt foil were placed in a customized Teflon reactor with air-equilibrated seawater (50 mL) in the absence or presence of U(VI) at varying pH values (3, 6, 8.2, and 10.4; unless otherwise specified, ~8.2). Potentials swept at a

scan rate of 50 mV s⁻¹ or constant potentials were applied to the CFO electrode using an electrochemical workstation (CompactStat, Ivium) in the dark or under simulated light of air mass 1.5 light (AM 1.5). A 150-W Xenon arc lamp (ABET Tech.) equipped with an AM 1.5 filter was used as the light source with a light intensity of 100 mW cm⁻² (1 sun), unless otherwise specified. Light was irradiated on the backside of the CFO electrodes (FTO side). If necessary, N₂ (>99.9%) was purged through the solution during experiments.

During the photoelectrochemical (PEC) experiments at constant potentials (-0.4, -0.5, and -0.6 V vs. SCE; hereafter SCE is omitted for simplicity, unless otherwise specified), aliquots (0.5 mL) were intermittently sampled for uranium analysis while recording currents. Quantification of U(VI) was completed using a spectrophotometric method with Arsenazo III ((HO)₂C₁₀H₂(SO₃H)₂(N=NC₆H₄AsO₃H₂)₂) as a chelating indicator of U(VI) [15]. This method has been shown to be accurate, reliable, and selective for hexavalent uranium [18,19], with no interference from seawater ions [20–22]. Details of the analytical method are described in the *Supplementary Information*. In addition, the total uranium remaining in seawater was quantified using inductively coupled plasma (ICP) spectrometry (Perkin Elmer, Optima 7300DV). The ICP standard solution of uranium (100 ± 10 ppm, GFS Chemicals) in 5% nitric acid was used for the measurements. To examine the oxidation states of uranium in solution, hydrous titania adsorbents with a high surface area (>300 m² g⁻¹) were prepared following a literature procedure [15]. The Faradaic efficiency of U(VI) conversion was estimated using the following equation:

$$\text{Faradaic efficiency (\%)} = \frac{[\text{U}^{(6-n)+}] (\text{mol}) \times n}{\text{total current (A)} \times \text{time (s)}} \times F \times 100$$

where, U⁽⁶⁻ⁿ⁾⁺ refers to uranium species with an oxidation state of (6 - n)+, n is the number of electrons, and F is the Faraday constant (96,485 C mol⁻¹).

2.3. Surface characterization

The surface morphology and composition of CFO were analyzed by field emission scanning electron microscopy (FE-SEM, Hitachi S-4800) equipped with energy-dispersive X-ray spectroscopy (EDS). The crystalline patterns of CFO were examined by X-ray diffraction (XRD, Rigaku D/Max-2500). The electrophoretic mobilities of CFO particles collected from the as-synthesized electrodes were measured to estimate their zeta potentials as a function of pH using an electrophoretic light scattering spectrometer (Zetasizer, Malvern) equipped with a He-Ne laser and thermostated flat board cell [23].

3. Results and discussion

3.1. Photocatalyst characterization

As-fabricated CFO films possessed a porous, double-layer structure with a ~0.5 μm thick underlayer and a ~3 μm thick porous overlayer (Fig. 1a). A uniformly formed underlayer acted as a seed layer, on which particles grew and interconnected, creating a blossom-like porous morphology (Fig. 1b). This double-layer configuration is unique, particularly in aqueous electrodeposition processes [16]. EDS analysis indicates that Cu and Fe were deposited simultaneously (Fig. 1c) and that their composition was uniform over the entire surface (Fig. 1d–f). However, the atomic ratio of Cu and Fe was not stoichiometric (Cu/Fe = ~1.55; see Fig. S1), suggesting that the synthesized sample was not a pure spinel (*e.g.*, CuFe₂O₄) or delafossite (*e.g.*, CuFeO₂). XRD characterization of the as-fabricated CFO films was performed to examine their crystalline structure (Fig. 2). Most of the XRD peaks were assigned

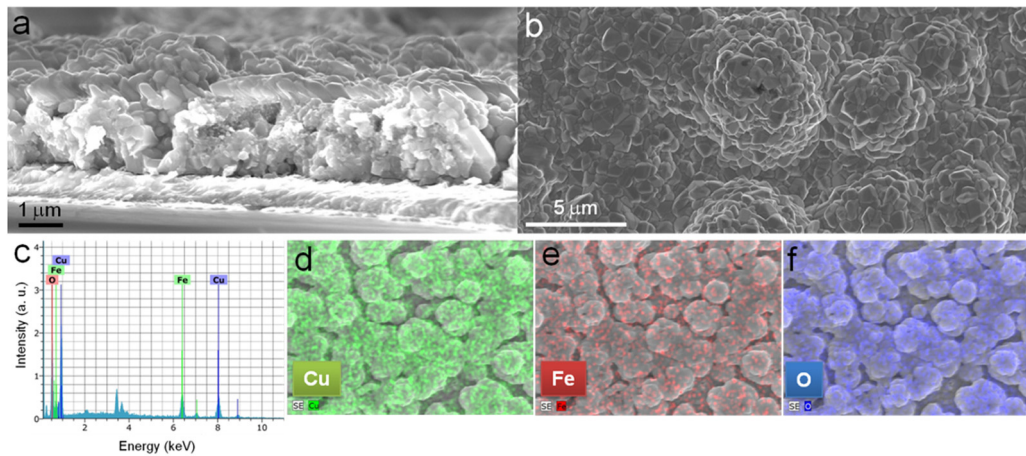


Fig. 1. SEM images of CuO/CuFeO₂ samples: (a) side view and (b) top view. EDS results for the elemental composition of CuO/CuFeO₂: (d) Cu, (e) Fe, and (f) O.

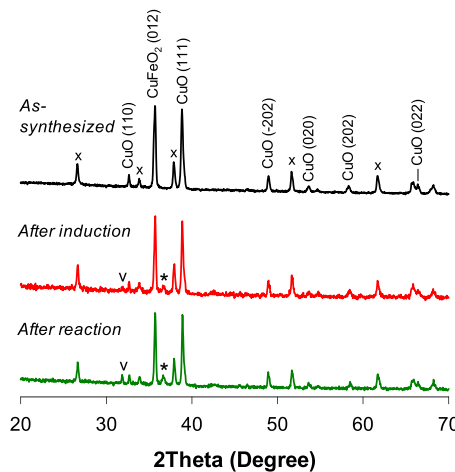


Fig. 2. XRD characterizations of CuO/CuFeO₂ samples synthesized and used for uranium conversion (~30 and 90 min for after induction and after reaction, respectively). For the induction, see text. Symbols "v" and "*" refer to newly generated peaks associated to NaCl and Cu₂O (111), respectively, whereas "x" indicates XRD peaks originated from FTO substrates.

to CuO (110, 111, 202, 020, 022, etc.) and a well-crystallized CuFeO₂ peak (012) was also found. CuO formation was attributed to oxidative annealing of the deposited Cu(II) precursor, while the presence of CuFeO₂ suggests that a fraction of Cu(II) was reduced to Cu(I) ($E^\circ(Cu^{2+}/Cu^+) = +0.16$ V vs. NHE). In contrast, Fe(III) remained unchanged ($E^\circ(Fe^{3+}/Fe^{2+}) = +0.77$ V vs. NHE) during the electrodeposition process [24]. Accordingly, CuFeO₂ was obtained by annealing the as-deposited sample under an O₂-free atmosphere. However, electrodeposition of Cu(II) alone and subsequent oxidative annealing led to CuO formation. All surface characterization results were consistent with those reported elsewhere [16], indicating the formation of heterojunction CFO.

3.2. Photoelectrochemical U(VI) conversion

Fig. 3a shows cyclic voltammograms of as-fabricated CFO electrodes in natural seawater without and with U(VI). In the absence of U(VI), broad anodic peaks appeared at approximately -0.05 V, with relatively small cathodic peaks at approximately -0.5 V (Fig. S2). The latter was associated with mixed reductions of Cu(II) (ca. -0.4 V) and Cu(I) (ca. -0.45 V) (Fig. 3a inset), whereas there was no obvious reduction peak of Fe(III). Accordingly, the significant anodic peaks should result from the oxidation of Cu(I) which is

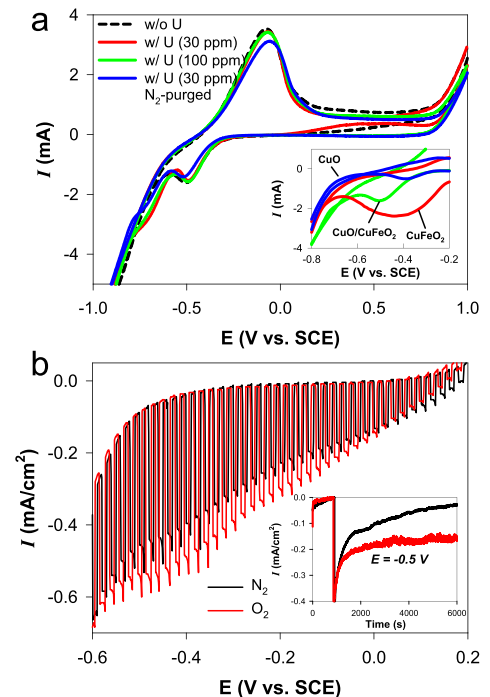


Fig. 3. (a) Cyclic voltammograms of CuO/CuFeO₂ electrodes in air-equilibrated seawater without (w/o) and with (w/) U(VI) (30 or 100 ppm). N₂ gas was purged into seawater to remove dissolved oxygen, if necessary. Inset compares voltammograms with CuO, CuFeO₂, and CuO/CuFeO₂ in seawater (without uranium). (b) Light-chopped linear sweep voltammograms of CuO/CuFeO₂ in seawater without and with N₂-purging. Inset shows time-profiled photocurrents at E = -0.5 V (black lines: N₂-purged; red lines: air-equilibrated). (For interpretation of the references to colour in this figure legend, the reader is referred to the web version of this article.)

both produced in the cathodic potential scan and originally present in CuFeO₂. The Fe^{3+/2+} redox reaction contribution was excluded due to the absence of new peaks in the cathodic scan of CuFeO₂ (Fig. 3a inset) and the low content of Fe compared with Cu (Fig. S1). No Cu⁰ was found in our previous study [16]; hence the redox reaction of Cu^{1+/0} was also not considered. The presence of uranium (30 and 100 ppm) hardly influenced the magnitude and position of anodic and cathodic peaks, and did not generate new reduction peaks. This indicates that the interaction between uranium and the surface was limited, and that direct electron transfer from the surface to uranium was unlikely to occur. When N₂ was purged through seawater containing U(VI) at 30 ppm, no significant change in the voltammogram was observed. However, a close

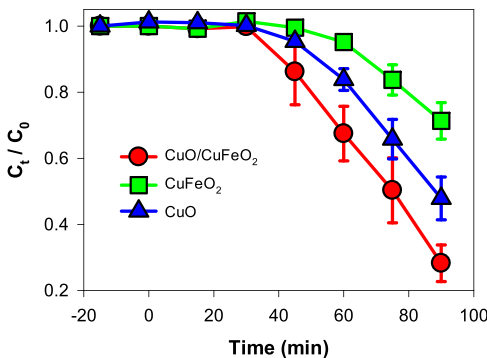
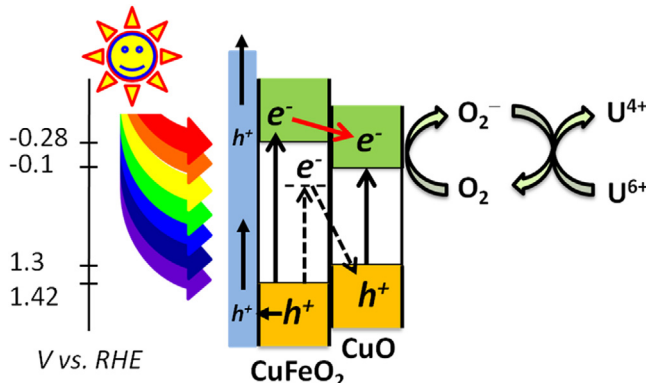


Fig. 4. Time-profiled changes in seawater U(VI) concentrations ($C_0 = 30$ ppm) using different photoelectrodes (CuO, CuFeO₂, and CuO/CuFeO₂) held at $E = -0.5$ V vs. SCE under simulated sunlight (AM 1.5; 100 mW cm⁻²). Samples were left in the uranium solution for >15 min prior to irradiation.



Scheme 1. U(VI) conversion process driven by CuO/CuFeO₂ photocathodes in seawater.

comparison shows that O₂ removal, by purging with N₂, shifted the peak by ~20 mV (Fig. S2), suggesting the involvement of dissolved O₂ at $E = ca.$ -0.5 V. In the photoelectrochemical study, light-chopped linear sweep voltammograms of ClO electrodes were examined in seawater purged with N₂ or O₂ (Fig. 3b). The onset potential (E_{on}) was *ca.* +0.2 V and the dark current flowed from $E < -0.35$ V owing to Cu(II) reduction. With O₂ or air-purging, the onset potential and dark current were insignificantly affected, whereas the photocurrents were obviously enhanced (Fig. S3). This suggests that O₂ was an effective electron acceptor, leading to efficient charge separation and facilitating hole transfer [16,24].

The three photocathodes, CFO (CuO/CuFeO₂), CuO, and CuFeO₂, were compared for their U(VI) conversion under simulated sunlight (AM 1.5; 100 mW cm⁻²) (Fig. 4). Clearly, the concentration of U(VI) decreased with irradiation time, while the conversion kinetics were different among the three electrodes, with CFO showing the best performance. The U(VI) conversion mechanism appeared to be virtually identical among the photocathodes, with the fastest conversion for CFO attributed to the heterojunction between CuO and CuFeO₂ (see Scheme 1). CuFeO₂, with an optical bandgap of *ca.* 1.05 eV, was reported to have several interband transitions working as charge trap (*i.e.*, recombination) sites [25,26]. When coupled with CuO (bandgap, *ca.* 1.4 eV), such recombination was shown to be significantly inhibited owing to the cascaded charge transfer at the CuO/CuFeO₂ interface [16]. Interestingly, induction times (*ca.* 30 min) were present in the uranium conversion, irrespective of the photocathode (Fig. 4). A control experiment showed insignificant uranium adsorption on the electrode surface, indicating that this induction time was not attributed to uranium adsorption. An

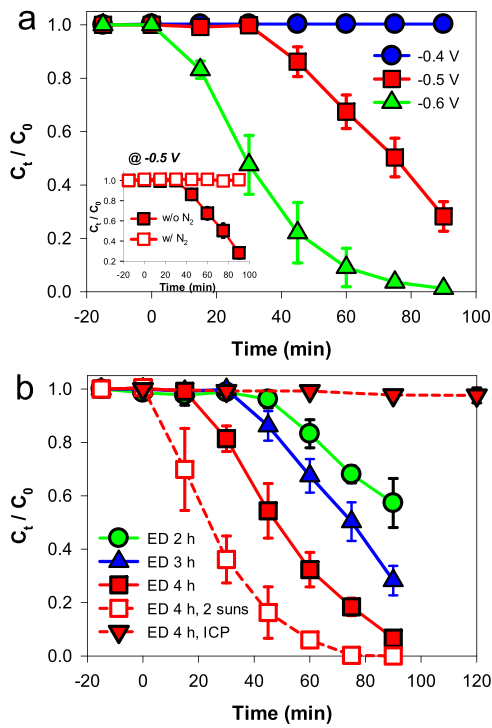


Fig. 5. (a) Time-profiled changes in seawater U(VI) concentration ($C_0 = 30$ ppm) with CuO/CuFeO₂ held at various potentials ($E = -0.4$, -0.5, and -0.6 V vs. SCE) under simulated sunlight (AM 1.5; 100 mW cm⁻²). Inset shows the effect of O₂ removal (*via* N₂-purging) on U(VI) concentration change at $E = -0.5$ V vs. SCE under AM 1.5 light. Samples were left in the uranium solution for >15 min prior to irradiation. (b) Effect of electrodeposition (ED) time (2, 3, and 4 h) of CuO/CuFeO₂ on U(VI) concentration changes under simulated sunlight (AM 1.5; 100 mW cm⁻²). If necessary, a stronger light (2 suns; 200 mW cm⁻²) was employed (ED 4 h, 2 suns). ICP refers to the total uranium in solution quantified by ICP spectrometry (ED 4 h, ICP).

induction time was not found when using TiO₂ as the photocathode in our previous study [15].

The PEC conversion of U(VI) was studied more systematically on irradiated CFO electrodes as a function of applied potentials (-0.4, -0.5, and -0.6 V) (Fig. 5a). At $E = -0.4$ V, adsorption and PEC conversion of U(VI) were insignificant. At $E = -0.5$ V, conversion of U(VI) started after 30 min of irradiation, while at $E = -0.6$ V it started immediately after irradiation. When purged with N₂ to remove dissolved O₂, uranium conversion at $E = -0.5$ V was significantly inhibited (Fig. 5a inset). In addition, the application of $E = -0.5$ V without irradiation did not change the uranium concentration (data not shown), suggesting that uranium conversion resulted absolutely from reaction with photogenerated electrons. The effects of electrodeposition (ED) time and irradiation intensity were also examined (Fig. 5b). With increasing ED time (2, 3, and 4 h), uranium conversion was enhanced and induction time decreased gradually (*ca.* 40, 30, and 15 min, respectively) under the condition of $E = -0.5$ V and a light intensity of 100 mW cm⁻² (1 sun) (Fig. 5b). With a light intensity of 200 mW cm⁻² (2 suns) U(VI) was converted immediately after irradiation (*i.e.*, no induction time; curve ED 4 h, 2 suns).

It is noteworthy that while ~95% of U(VI) (initially 30 ppm) was converted within 90 min, the total amount of uranium in seawater remained unchanged during the same period (curve ED 4 h, ICP in Fig. 5b). This indicates that virtually all conversion reactions of U(VI) occurred in the bulk solution, and that the surface reaction (direct electron transfer from the surface to the adsorbed uranium) was limited due to insignificant adsorption of U(VI). It was presumed that U(VI) conversion occurred indirectly with O₂, which mediated between photogenerated electrons on the surface and U(VI) in the

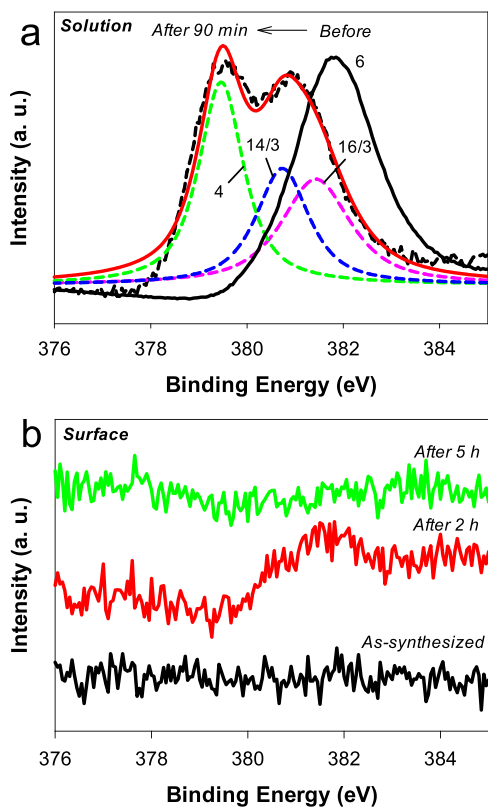


Fig. 6. XPS U4f_{7/2} band analysis of uranium in (a) seawater and (b) CuO/CuFeO₂ before and after photoelectrochemical reactions ($E = -0.5$ V vs. SCE; AM 1.5 light; 1 sun; air-equilibrated). In (a), numbers refer to uranium oxidation states.

bulk. This presumption was confirmed when removal of O₂ by N₂ purging completely inhibited U(VI) conversion (Fig. 5a inset; see below for conversion mechanism).

To examine the changes in the oxidation states of U(VI), the uranium in solution was collected after reacting for 90 min and oxidation states analyzed by XPS (Fig. 6a). A uranium band (U4f_{7/2}) was found in the range 379.6–380.9 eV, which overlapped with two or more sub-bands. The overall binding energy was smaller than that of U⁶⁺ (uranyl nitrate, centered at ~381.9 eV) by 1–2 eV, indicating the conversion of U⁶⁺ to lower oxidation states. The uranium band was further resolved to gain insight into the uranium oxidation states. Three oxidation states (+4, +14/3, and +16/3) were observed, with a percentage ratio of 42:28:30 (i.e., UO₂, U₃O₇, and U₃O₈, respectively, assuming uranium was coordinated to oxygen). In addition, the CFO surface (as synthesized and used for 2 and 5 h for PEC U(VI) conversion) was analyzed by XPS (Fig. 6b). The as-synthesized sample did not show any uranium-related XPS band (i.e., U4f_{7/2}), while CFO used for 2 h exhibited a trace signal. The uranium peak was not present in the sample used for 5 h. Accordingly, virtually all uranium (30 ppm) should be present in solution. Based on this distribution, the Faradaic efficiency of U(VI) conversion was estimated by dividing the number of electrons required for each uranium species (0.51, 0.23, and 0.12C for UO₂, U₃O₇, and U₃O₈, respectively) by the total number of electrons flowed ($0.88 \pm 0.02C$) (see Eq. (1) for estimation and Fig. 3b inset for currents). The overall Faradaic efficiency was ~98%, which suggests that virtually all photogenerated electrons were used for U(VI) conversion.

3.3. Uranium photoconversion mechanism

For effective uranium conversion, the photogenerated electrons need to be efficiently injected into U(VI). A previous study with TiO₂

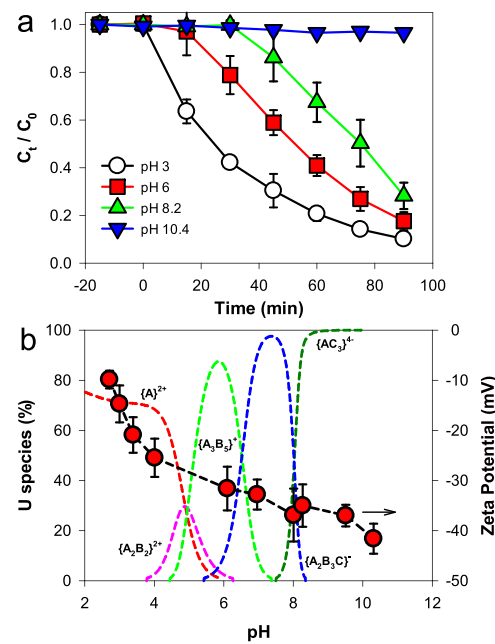


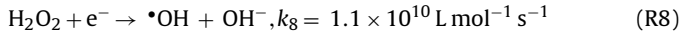
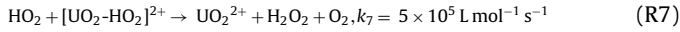
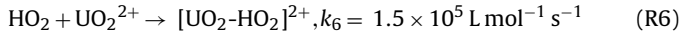
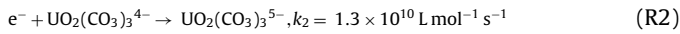
Fig. 7. (a) Effect of pH value (3, 6, 8.2, and 10.4) on U(VI) concentration changes with CuO/CuFeO₂ under simulated sunlight (AM 1.5; 100 mW cm⁻²; air-equilibrated). (b) pH-dependent speciation of U(VI) and zeta potentials of CuO/CuFeO₂ particles. A, B, and C refer to UO₂, OH, and CO₃, respectively (e.g., $\{A_2B_3C\}^- = UO_2(OH)_3CO_3^-$). For simplicity, other minor species (UO_2F^+ , UO_2Cl^+ , UO_2OH^+ , and $UO_2(CO_3)_2^{2-}$) were not shown. For the uranium speciation, see Ref. [15].

presumed that dissolved O₂ was the primary electron acceptor in air-equilibrated seawater at pH 8.2, while mediating the photo-generated electrons between TiO₂ and uranium (Scheme 1) [15]. However, in this study, the suggested mechanism could not fully explain the presence of an induction time (~30 min under typical experimental conditions), because, with O₂ as the electron mediator, uranium conversion should initiate soon after irradiation. H₂O₂ was not produced, and hence we excluded the possibility of an induction time for H₂O₂ formation via O₂ reduction (i.e., O₂ + 2H⁺ + 2e⁻ → H₂O₂).

To gain further insight into the mechanism, the effect of pH on uranium conversion was examined (Fig. 7a). Whereas uranium conversion was very limited at pH 10.4, a decrease in pH enhanced uranium conversion and shortened the induction time. For example, at pH 6, the conversion initiated with induction time of ~15 min. In contrast, there was no induction time perceived at pH 3, with uranium conversion occurring immediately after irradiation. This tendency was in contrast to the result of our previous study, in which uranium was not converted at pH 3 with a TiO₂ photoelectrode [15]. It is noteworthy that U(VI) exists as diverse species as a function of pH, particularly in seawater containing (bi)carbonate. As shown in Fig. 7b, the primary species of U(VI) at pH > ~9 and pH < ~4 are $UO_2(CO_3)_3^{4-}$ and UO_2^{2+} , respectively. According to this speciation plot, all U(VI) species exist as cations at pH < ~6 and as anions at pH > ~7.5. For comparison, pH-dependent zeta potentials of CFO particles are also shown. In the pH range 2–11, CFO possessed negative surface charges, while the zeta potentials became more negative with increasing pH.

A comparison of the U(VI) species and CFO surface charge is informative for speculating the uranium conversion mechanism. Under acidic conditions (pH < 6), U(VI) can approach the electrode surface via electrostatic attraction and accept photogenerated electrons readily from the surface. Although uranium is not chemically adsorbed to the surface, such a reduction of U(VI) by the photogenerated electron would occur across the double layer. Taking into account that the reaction rate between the aqueous electron

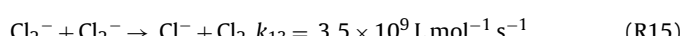
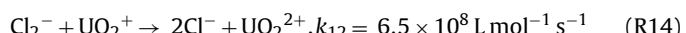
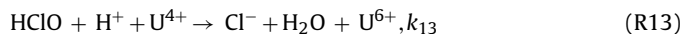
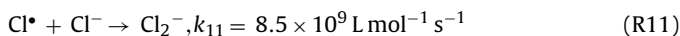
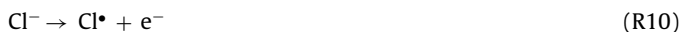
and U(VI) (e.g., UO_2^{2+} and $\text{UO}_2(\text{CO}_3)_3^{4-}$) is diffusion-limited, with a bimolecular rate constant of $\sim 10^{10} \text{ L mol}^{-1} \text{ s}^{-1}$ [27] (R1 and R2, respectively), direct electron transfer might lead to the absence (or minimization) of induction time in U(VI) conversion at pH 3 (Fig. 7a).



Under these conditions, the role of O_2 as an electron mediator is very limited. If the superoxide radical anion ($\text{O}_2^{\bullet-}$) has a key role (R3 and R4) at pH 3, then the U(VI) conversion must be retarded, because a significant fraction of superoxide radical anions would change to hydroperoxide (HO_2) ($pK_a = 4.8$; see R5). The reaction of HO_2 with U(VI) (i.e., UO_2^{2+} at pH 3) is as slow as $10^5 \text{ M}^{-1} \text{ s}^{-1}$ (R6) and further inhibited by additional HO_2 (R7) owing to a slightly faster reaction compared with R6. As R7 continues, H_2O_2 accumulates and decomposes to hydroxyl radicals (R8) that can re-oxidize the reduced uranium (R9).

Increasing pH above 6 induces electrostatic repulsion, while inhibiting direct electron transfer at the CFO/solution interface. Under these conditions, O_2 can mediate electron transfer and reduce U(VI) (R3 and R4). To explain the presence of induction time, we presumed that the electrodes held the photogenerated electrons somehow, then releasing them to O_2 after a certain period of time. We compared XRD patterns of CuO/CuFeO₂ electrodes (as-fabricated, after an induction time of ~30 min and a reaction time of 90 min) (Fig. 2). The three samples showed the same crystalline pattern, except for two new peaks at $2\theta = 31.84^\circ$ and 36.64° in the latter two samples. Whereas the former peak resulted from NaCl, the latter peak was attributed to the Cu_2O (111) peak, which was stronger in the sample used for 90 min. This suggests that CuO/CuFeO₂ undergoes partial reduction (Cu^{2+} to Cu^+) caused by photogenerated electrons and subsequent transformation into unwanted ternary CuO/ Cu_2O /CuFeO₂. After a certain period of time, the electrode self-optimizes with regard to composition and begins electron transfer to O_2 . It should be noted that the deformation of CuO/CuFeO₂ can be thermally healed by recycling the used samples via oxidative annealing [28].

The oxidation of reduced uranium by reactive chlorine species (RCS, including Cl_2^- and HOCl) could be an alternative mechanism (R10–R15) to give the induction time. They are typically found in the oxidation of aqueous chloride at concentrations of >ca. 20 mM (cf. $[\text{Cl}^-]_{\text{seawater}} \sim 0.5 \text{ M}$) [29–33], while longer-lived than $\cdot\text{OH}$. Unfortunately, a kinetics comparison between the uranium reduction reaction by $\text{O}_2^{\bullet-}$ (R4) and the oxidation reaction by RCS (e.g., R14) was difficult due to the k_4 value being unavailable. The existence of an induction time merely implies that R14 is comparable to R4 in the initial stage, and gradually less dominant as dichloride radical anions are decomposed via disproportionation (R15).



While the partial reduction of CFO electrodes and the Cl_2^- -mediated oxidation pathway both lead to an induction time, the latter appears to be predominant. The contribution of HOCl to the uranium oxidation appeared to be insignificant because of lower oxidation power compared with Cl_2^- ($E^\circ(\text{Cl}_2^-/\text{Cl}^-) = 2.0 \text{ V}$; $E^\circ(\text{HOCl}/\text{Cl}^-) = 1.49 \text{ V}$).

4. Conclusions

We have demonstrated that mixed CuO and CuFeO₂ photoelectrodes successfully reduce U(VI) to a lower oxidation state (+4, +14/3, and +16/3) in air-equilibrated seawater. The overall Faradaic efficiency of uranium reduction was ~98% at a constant potential of –0.5 V to the CuO/CuFeO₂ electrode, and the performance of the mixed electrode was higher than that of either CuO or CuFeO₂. All the conversion reactions of U(VI) occurred predominantly in the bulk solution; surface reactions (direct electron transfers from the surface to adsorbed uranium) were limited because of insignificant adsorption of U(VI) in the circum-neutral pH range. Under these conditions, O_2 acted as an electron shuttle between the electrodes and U(VI). With the removal of O_2 , uranium conversion failed to occur. The observed induction time for uranium conversion was attributed to the partial reduction of CuO/CuFeO₂ electrodes and a reactive chlorine species-mediated oxidation pathway.

Acknowledgements

This research was supported by the Global Research Network Program (2014S1A2A2027802), Basic Science Research Program (2016R1A2B4007366), Space Core Technology Development Program (2014MA3A3A02034875), and Nano-Material Technology Development Program (2016M3A7B4908169) through the National Research Foundation, Korea. In addition, we are grateful to the Korea CCS R&D Center (KCRC) (No. 2014M1A8A1049354) for financial support. This publication was made possible by a grant from the Qatar National Research Fund under its National Priorities Research Program (NPRP 7-865-2-320).

Appendix A. Supplementary data

Supplementary data associated with this article can be found, in the online version, at <http://dx.doi.org/10.1016/j.apcatb.2017.02.004>.

References

- [1] D. Cui, J. Low, K. Spahiu, Environmental behavior of spent nuclear fuel and canister materials, *Energy Environ. Sci.* 4 (2011) 2537–2545.
- [2] R.C. Ewing, Nuclear fuel cycle: environmental impact, *MRS Bull.* 33 (2008) 338–340.
- [3] J. Kim, C. Tsouris, R.T. Mayes, Y. Oyola, T. Saito, C.J. Janke, S. Dai, E. Schneider, D. Sachde, Recovery of uranium from seawater: a review of current status and future research needs, *Sep. Sci. Technol.* 48 (2013) 367–387.
- [4] D.L. Clark, D.E. Hobart, M.P. Neu, Actinide carbonate complexes and their importance in actinide environmental chemistry, *Chem. Rev.* 95 (1995) 25–48.
- [5] K. Maher, J.R. Bargar, G.E. Brown Jr., Environmental speciation of actinides, *Inorg. Chem.* 52 (2013) 3510–3532.
- [6] K. Kusakabe, A. Goto, S. Morooka, Kinetics of uranium adsorption from seawater with imidodioxime adsorbent, *Sep. Sci. Technol.* 29 (1994) 1567–1577.
- [7] R.V. Davies, J. Kennedy, K.M. Hill, R.W. McIlroy, R. Spence, Extraction of uranium from sea water, *Nature* 203 (1964) 1110–1115.
- [8] M.J. Comarmond, T.E. Payne, J.J. Harrison, S. Thiruvoth, H.K. Wong, R.D. Augherson, G.R. Lumpkin, K. Mueller, H. Foerstendorf, Uranium sorption on

various forms of titanium dioxide: influence of surface area, surface charge, and impurities, *Environ. Sci. Technol.* 45 (2011) 5536–5542.

[9] A. Zhang, G. Uchiyama, T. Asakura, pH effect on the uranium adsorption from seawater by a macroporous fibrous polymeric material containing amidoxime chelating functional group, *React. Funct. Polym.* 63 (2005) 143–153.

[10] B. Ahmed, B. Cao, B. Mishra, M.I. Boyanov, K.M. Kemner, J.K. Fredrickson, H. Beyenal, Immobilization of U(VI) from oxic groundwater by Hanford 300 Area sediments and effects of Columbia River water, *Water Res.* 46 (2012) 3989–3998.

[11] R. Amadelli, A. Maldotti, S. Sostero, V. Carassiti, Photodeposition of uranium-oxides onto TiO₂ from aqueous uranyl solutions, *J. Chem. Soc. Faraday Trans.* 87 (1991) 3267–3273.

[12] J. Chen, D.F. Ollis, W.H. Rulkens, H. Bruning, Photocatalyzed deposition and concentration of soluble uranium(VI) from TiO₂ suspensions, *Colloid Surf. A* 151 (1999) 339–349.

[13] V. Eliet, G. Bidoglio, Kinetics of the laser-induced photoreduction of U(VI) in aqueous suspensions of TiO₂ particles, *Environ. Sci. Technol.* 32 (1998) 3155–3161.

[14] S.O. Odoh, Q.J. Pan, G.A. Shamov, F.Y. Wang, M. Fayek, G. Schreckenbach, Theoretical study of the reduction of uranium(VI) aquo complexes on titania particles and by alcohols, *Chem.-Eur. J.* 18 (2012) 7117–7127.

[15] Y.K. Kim, S. Lee, J. Ryu, H. Park, Solar conversion of seawater uranium (VI) using TiO₂ electrodes, *Appl. Catal. B* 163 (2015) 584–590.

[16] U. Kang, S.K. Choi, D.J. Ham, S.M. Ji, W. Choi, D.S. Han, A. Abdel-Wahab, H. Park, Photosynthesis of formate from CO₂ and water at 1% energy efficiency via copper iron oxide catalysis, *Energy Environ. Sci.* 8 (2015) 2638–2643.

[17] N.C. Deb Nath, S.Y. Choi, H.W. Jeong, J.-J. Lee, H. Park, Stand-alone photoconversion of carbon dioxide on copper oxide wire arrays powered by tungsten trioxide/dye-sensitized solar cell dual absorbers, *Nano Energy* 25 (2016) 51–59.

[18] S.B. Savvin, Analytical use of arsenazo III. Determination of thorium zirconium, uranium and rare earth elements, *Talanta* 8 (1961) 673–685.

[19] H. Rohwer, N. Rheeder, E. Hosten, Interactions of uranium and thorium with arsenazo III in an aqueous medium, *Anal. Chim. Acta* 341 (1997) 263–268.

[20] M.H. Khan, P. Warwick, N. Evans, Spectrophotometric determination of uranium with arsenazo-III in perchloric acid, *Chemosphere* 63 (2006) 1165–1169.

[21] T. Nakashima, K. Yoshimura, T. Taketatsu, Determination of uranium(VI) in seawater by ion-exchanger phase absorptiometry with arsenazo III, *Talanta* 39 (1992) 523–527.

[22] T.M. Bhatti, A. Mateen, M. Amin, K.A. Malik, A.M. Khalid, Spectrophotometric determination of uranium(VI) in bacterial leach liquors using arsenazo-III, *J. Chem. Technol. Biotechnol.* 52 (1991) 331–341.

[23] H. Park, W. Choi, Effects of TiO₂ surface fluorination on photocatalytic reactions and photoelectrochemical behaviors, *J. Phys. Chem. B* 108 (2004) 4086–4093.

[24] C.G. Read, Y. Park, K.S. Choi, Electrochemical synthesis of p-type CuFeO₂ electrodes for use in a photoelectrochemical cell, *J. Phys. Chem. Lett.* 3 (2012) 1872–1876.

[25] F.A. Benko, F.P. Koffyberg, Opto-electronic properties of p- and n-type delafossite, CuFeO₂, *J. Phys. Chem. Solids* 48 (1987) 431–434.

[26] S. Omeiri, B. Bellal, A. Bouguelia, Y. Bessekhouad, M. Trari, Electrochemical and photoelectrochemical characterization of CuFeO₂ single crystal, *J. Solid State Electrochem.* 13 (2009) 1395–1401.

[27] G.V. Buxton, C.L. Greenstock, W.P. Helman, A.B. Ross, Critical review of rate constants for reactions of hydrated electrons, hydrogen atoms and hydroxyl radicals (OH/O[·]) in aqueous solution, *J. Phys. Chem. Ref. Data* 17 (1988) 513–886.

[28] U. Kang, H. Park, A facile synthesis of CuFeO₂ and CuO composite photocatalyst films for production of liquid formate from CO₂ and water over a month, *J. Mater. Chem. A* (2017), <http://dx.doi.org/10.1039/C1036TA09378G>.

[29] J. Kim, W.J.K. Choi, J. Choi, M.R. Hoffmann, H. Park, Electrolysis of urea and urine for solar hydrogen, *Catal. Today* 199 (2013) 2–7.

[30] S. Kim, S.K. Choi, B.Y. Yoon, S.K. Lim, H. Park, Effects of electrolyte on the electrocatalytic activities of RuO₂/Ti and Sb-SnO₂/Ti anodes for water treatment, *Appl. Catal. B* 97 (2010) 135–141.

[31] H. Park, C.D. Vecitis, M.R. Hoffmann, Electrochemical water splitting coupled with organic compound oxidation: the role of active chlorine species, *J. Phys. Chem. C* 113 (2009) 7935–7945.

[32] S.Y. Yang, D. Kim, H. Park, Shift of the reactive species in the Sb-SnO₂-electrocatalyzed Inactivation of e-coli and degradation of phenol: effects of nickel doping and electrolytes, *Environ. Sci. Technol.* 48 (2014) 2877–2884.

[33] Y.Y. Ahn, S.Y. Yang, C. Choi, W. Choi, S. Kim, H. Park, Electrocatalytic activities of Sb-SnO₂ and Bi-TiO₂ anodes for water treatment: effects of electrocatalyst composition and electrolyte, *Catal. Today* 282 (2017) 57–64.